WSRC-MS-99-00078

Microstructural Characterization of 6061 Aluminum to 304L Stainless Steel Inertia Welds

K. A. Dunn, M. R. Louthan, and M. H. Tosten
Westinghouse Savannah River Company
Aiken, SC 29808

M. L. Birt
Auburn University
Auburn, Alabama

Abstract

Microstructural characterization of 6061-T6 aluminum-to-Type 304L stainless steel inertia welds provided a technical basis to conclude that transition joints fabricated from such welds should satisfactorily contain helium/hydrogen gas mixtures. This conclusion is based on the lack of semi-continuous alignments of particles and/or inclusions at, or near, the aluminum-to-stainless steel interface. These dissimilar metal transition joints play a key role in the operation of an accelerator driven, spallation neutron source designed for the production of tritium. The Accelerator Production of Tritium system will produce tritium through neutron interactions with ^{3}He gas contained in water-cooled, 6061-T6 aluminum pressure tubes. Current design concepts include thousands of thin-walled pressure tubes distributed throughout a number of aluminum-clad, lead-filled, blanket modules. The aluminum pressure tubes are connected to a tritium extraction and purification system through a stainless steel manifold. The transition from aluminum to stainless steel is made via transition joints machined from the aluminum-to-stainless steel inertia welds. The paper describes the baseline microstructural characterization of the welds, including optical, scanning and transmission electron microscopy and uses that characterization to evaluate potential gas leakage across the weld.

Introduction

The Accelerator Production of Tritium (APT) project represents one of several concepts being evaluated as the potential tritium source necessary to meet the defense needs of the United States of America. Design, construction and operation of the, one-of-a-kind APT facility will involve the utilization of a wide variety of materials that are exposed to unique conditions, including a high-energy mixed proton and neutron spectra. The target/blanket portion of the APT system will contain components and structures that have design lifetimes that

range from approximately one to over forty years. Tritium will be produced through (n,p) interactions with ^{3}He gas that is contained at approximately 1MPa in pressure tubes fabricated from 6061-T6 aluminum. Thousands of these pressure tubes are distributed throughout the target/blanket system. The tubes are positioned vertically inside aluminum-clad lead blanket modules so that cooling water can pass along the outer tube surfaces. Each tube is connected to the tritium extraction and purification system through a series of stainless steel manifolds via a transition joint. The transition joint is machined from a 304 stainless steel to 6061-T6 aluminum inertia weld. Joint configuration is such that the aluminum side of the machined joint can be welded to the aluminum pressure tube and the stainless steel side can be welded into the stainless steel gas distribution manifold. Anticipated design lifetimes of the pressure tubes are typical of other components in the target/blanket system. Tubes closest to the tungsten targets will be replaced about once a year while the outer tubes should not require replacement. Containment of the helium and tritium gasses in the pressure tubes must be assured throughout the design life and several approaches have been used to develop the technical basis for that assurance.

The service life of the ^{3}He pressure tubes may be limited because of a variety of environmental degradation processes. These processes include: a) irradiation-induced losses in ductility and toughness, b) corrosion-induced losses in wall thickness and/or tube wall integrity, c) fatigue-induced crack growth, and d) synergistic effects among two or more degradation mechanisms. Each of these effects must be understood and accounted for as service lifetimes and replacement schedules are developed. The aluminum-to-stainless steel transition joint is a potential weak link for pressure tube integrity. This interface could provide a leak path for helium and/or tritium and the galvanic couple could accelerate corrosion to unacceptable levels. Additionally, there is little or no data describing the effects of irradiation at the transition joint. Therefore, an experimental program was established to validate the performance of the transition joint, and other APT target/blanket materials and components, under prototypical ATP operating conditions.

Assemblies, designed to evaluate the performance of materials and components for the APT target/blanket system, were irradiated in a mixed proton and neutron spectra in test Area-A of the Los Alamos Neutron science Center (LANSCE). Neutrons were generated by spallation reactions caused by interactions of the high-energy proton beam with a tungsten target assembly. The irradiated assemblies included several components that used the aluminum-to-stainless steel transition joints. The joints were irradiated while being exposed to cooling water, air and/or helium/tritium gas mixtures. Evaluation of the irradiated transition joints is currently underway. However, to provide a baseline for evaluating the irradiated transition joints, non-irradiated transition joints were characterized by optical and electron microscopy. Analysis of the distributions of particles at, or near, the weld interface provided a basis to assess the likelihood for weld-induced leak paths in the transition joints. The metallographic study also served to develop sample preparation techniques that were suitable for the hot-cell evaluations of the irradiated transition joints. This paper summarizes the results of the baseline evaluation.

Text

Inertia Weld Information

Inertia welding is a process that welds (or joins) two parts by the transfer of kinetic energy from a flywheel to the weld interface. One of the parts is attached to the flywheel and accelerated to a defined rotational speed while the other part is held stationary. When the flywheel and attached part obtain the required kinetic energy (rotational speed), the driving motor is disengaged and the assembly is allowed to rotate freely. The rotating assembly and stationary part are then pressed with an applied axial force [1]. Interfacial friction due to the relative rotation of the faying surfaces breaks up and/or removes surface films, heats the interfacial region and ultimately causes the contacting parts to bond. The resulting bond is termed an inertia weld.

Inertia welding usually results in short welding times, limited flash and narrow heat affected zones. The process is particularly useful for joining dissimilar metals [2]. The heat evolved while making the aluminum-to-stainless steel inertia welds evaluated in this study was sufficient to discolor the outer surfaces of the stainless steel sections (Figure 1). The time-temperature profiles vary with location across the weld interface (Figure 2). The

deposition of thermal energy is apparently a minimum at the sample center and a maximum somewhere between the center and the sample periphery.

The faying surfaces on both the aluminum and stainless steel rods were flat, except for a machined hole at the center of the steel rod. This hole provided an internal site for aluminum extrusion during the joining operation (Figure 1). The 6061-T6 aluminum rods used for the test welds had heterogeneous microstructures with the largest grains located near the rod centerline and the grain size decreasing toward the rod periphery (Figure 3). The aluminum grain size had no apparent effect on weld quality as might be anticipated because the welding operation caused plastic deformation and recrystallization of the aluminum near the aluminum-to-stainless steel weld interface.

The inertia welds were converted from rod sections into transition joints by machining the outer surfaces to form a right circular cylinder with the desired outer diameter and drilling through the rod center lines to form a pipe section with the desired wall thickness. The transition joints tested in the LANSCE irradiation were Gas Tungsten Arc (GTA) welded to the appropriate aluminum or stainless steel sections before testing. Five of the transition joints welded to ^{3}He pressure tubes and leak tested after being helium filled and prior to irradiation. Similar joints were given hydraulic burst tests to confirm weld quality. The hydraulically burst tested joints all failed in regions of the aluminum that were remote from the weld and heat affected zone [4]. Non-machined rod samples prepared from the heats of materials used for the transitions joints irradiated in LANSCE were used for the metallographic analysis.
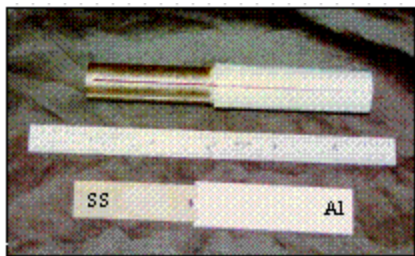

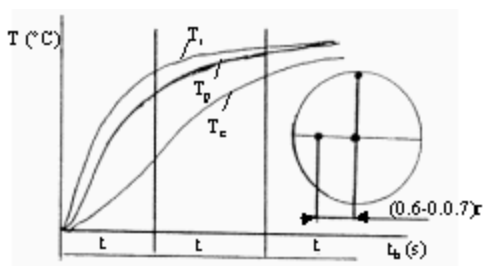**Figure 1. Inertia welded 304L stainless steel to 6061 T6 aluminum**

Figure 2. Temperature changes in material at various points during heating where T is temperature and t is time. (Note that T_p is periphery, T_c is center, and T_r is located at a point removed from the center at a distance of 0.6-0.7r.) [3]
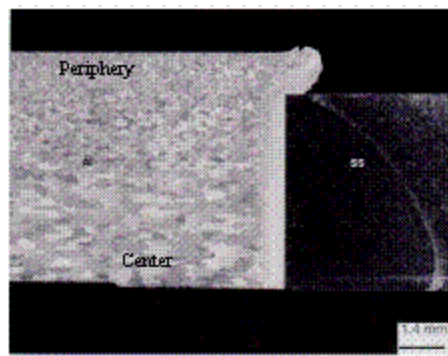
**Figure 3. Low magnification photograph of longitudinal cross section of
304L stainless steel to 6061 T6 aluminum inertia weld.**

Helium/Hydrogen Containment

Aluminum-to-stainless steel transition joints have been used in helium and hydrogen containment systems for over twenty five years. For example, test systems built in 1974 for measuring tritium permeation through aluminum alloys used an aluminum-to-stainless steel transition joint [5]. Tritium permeation measurements were made on the tubes by passing a sweep gas over the outer surface of the permeation tube. Permeability measurements with this apparatus were as low as 10^{-18} cc sec^{-1} cm^{-1} atm$^{-1/2}$. The sweep gas also passed over the transition joint and if tritium had leaked from the joint, low level permeation measurements could not have been made. The initial decision to use the aluminum-to-stainless steel transition joint in the APT target/blanket system was based on this type of experience.

The tubes irradiated in LANSCE were filled with 0.7 MPa ^{3}He. The ^{3}He-tube design and the use of the aluminum-to-stainless steel transition joint were similar to the earlier tritium permeation samples. The ^{3}He-tubes were made by welding a cap on one end of an aluminum pipe section and the transition joint to the other. A stainless steel fitting was welded to the stainless steel side of the transition joint. The fitting was used to pressurize the tube with ^{3}He. Pressurized tubes were sealed with a pinch weld on the stainless steel fitting. Filled tubes were then leak tested. Instrument sensitivity for the leak tests was <1.1E-9 STP cc ^{4}He/sec and no leakage was detected from any of the five tubes tested. The lack of detectable leakage across the transition joint welds was consistent with the results for the earlier tritium permeation experiments and demonstrated that the aluminum-to-stainless steel interface did not provide a significant pathway for gas leakage. Microstructural observations on similar aluminum-to-stainless steel interfaces supported the lack of an apparent leak path.

Specimen Preparation

Samples for baseline analysis were obtained from the Al/SS inertia welded rod by Electrical Discharge Machining (EDM) and sectioning with a standard cutting disk. This EDM cutting method removes material with spark erosion while a wire electrode moves through the material being machined. The electrode wire may be made of copper, tungsten, molybdenum, or brass. For this examination, brass wire was used.

A thin section along the length of the Al/SS rod was obtained by EDM. From this section, EDM was used to obtain disks with a diameter of approximately 3 mm of both the parent materials and at the Al/SS interface. Significant surface cavitation was observed on both the Al and SS following each EDM step. In addition, the SS section was also discolored following each machining step (Figures 1 and 4). A sample obtained by both the cutting wheel sectioning and EDM was analyzed with Scanning Electron Microscopy (SEM) to identify any effects the sectioning process might have on results from the study (Figure 4).
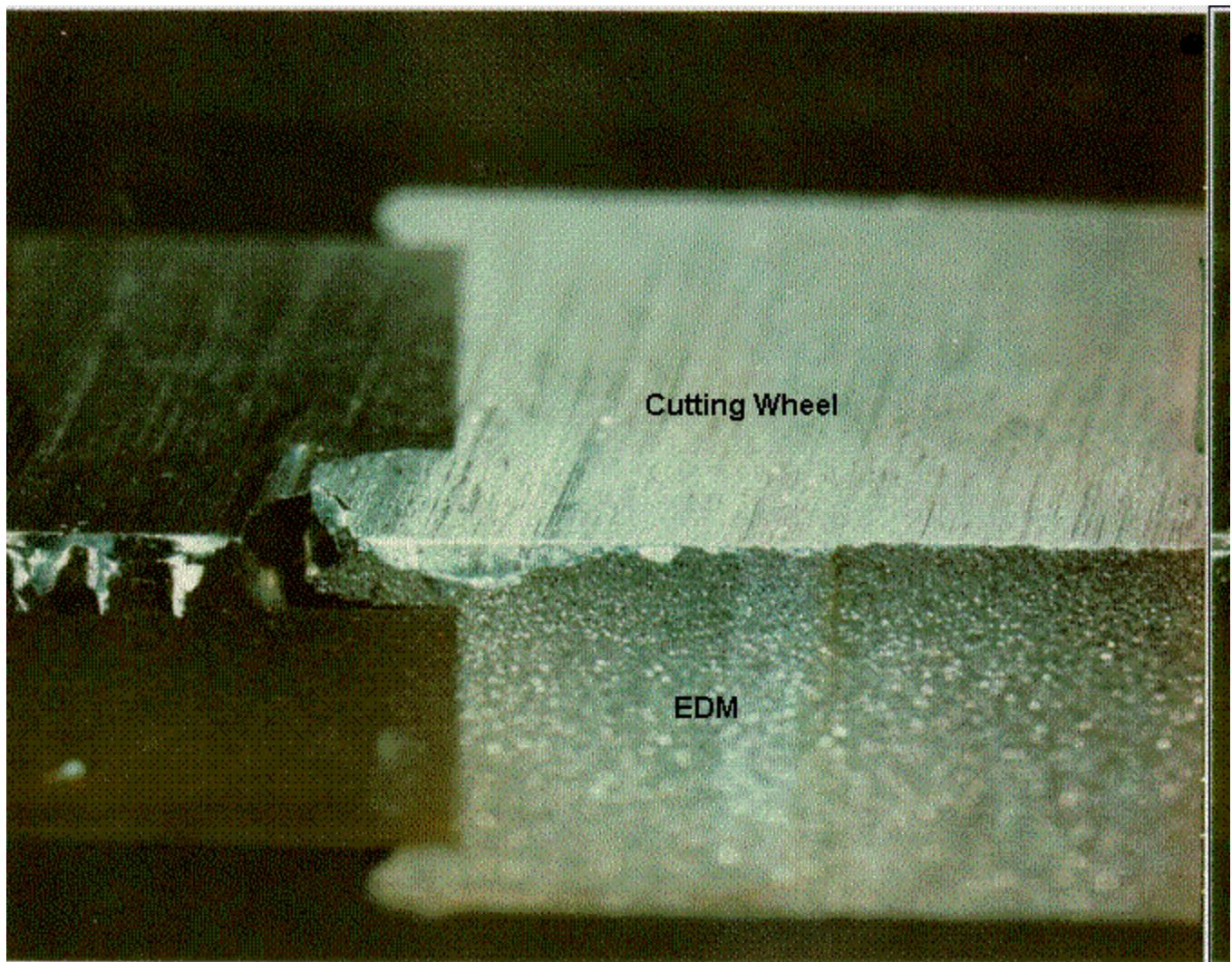
Figure 4. Quartered section of 304L stainless steel cut by both a cutting wheel and EDM.

SEM confirmed surface cavitation associated with EDM (Figure 5), and Energy Dispersive Spectroscopy (EDS) identified surface deposits remaining on both the Al and the SS as a result of the brass wire electrode (Figure 6). The EDS analysis indicated the presence of Cu and Zn on both the SS and the Al material. A similar EDS analysis of the surfaces exposed by the cutting wheel, Figure 7, yielded the expected plots for Al and SS, as shown in Figures 8 and 9. These inertia welded samples were mounted longitudinally and prepared metallographically. An EDS analysis of the metallographically prepared Al/SS weld sections did not indicate the presence of any brass wire deposits.
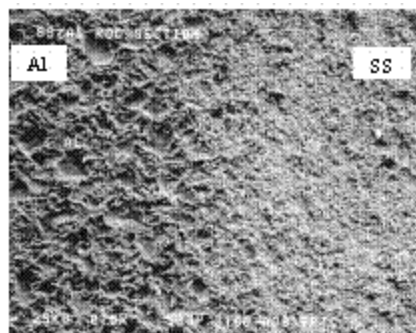
Figure 5. SEM photograph showing the surface cavitation resulting from the EDM process.
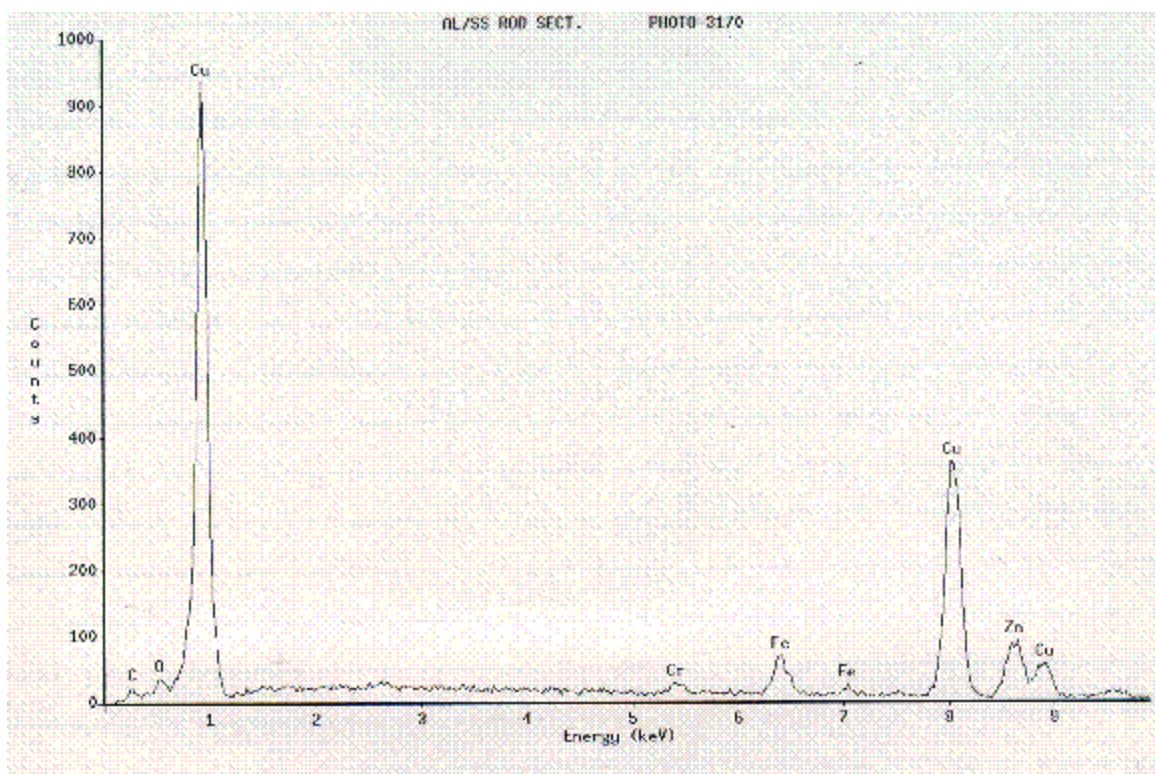

Figure 6. EDS analysis representative of Cu and Zn deposits on both the Al and the SS portions of the samples sectioned with EDM.
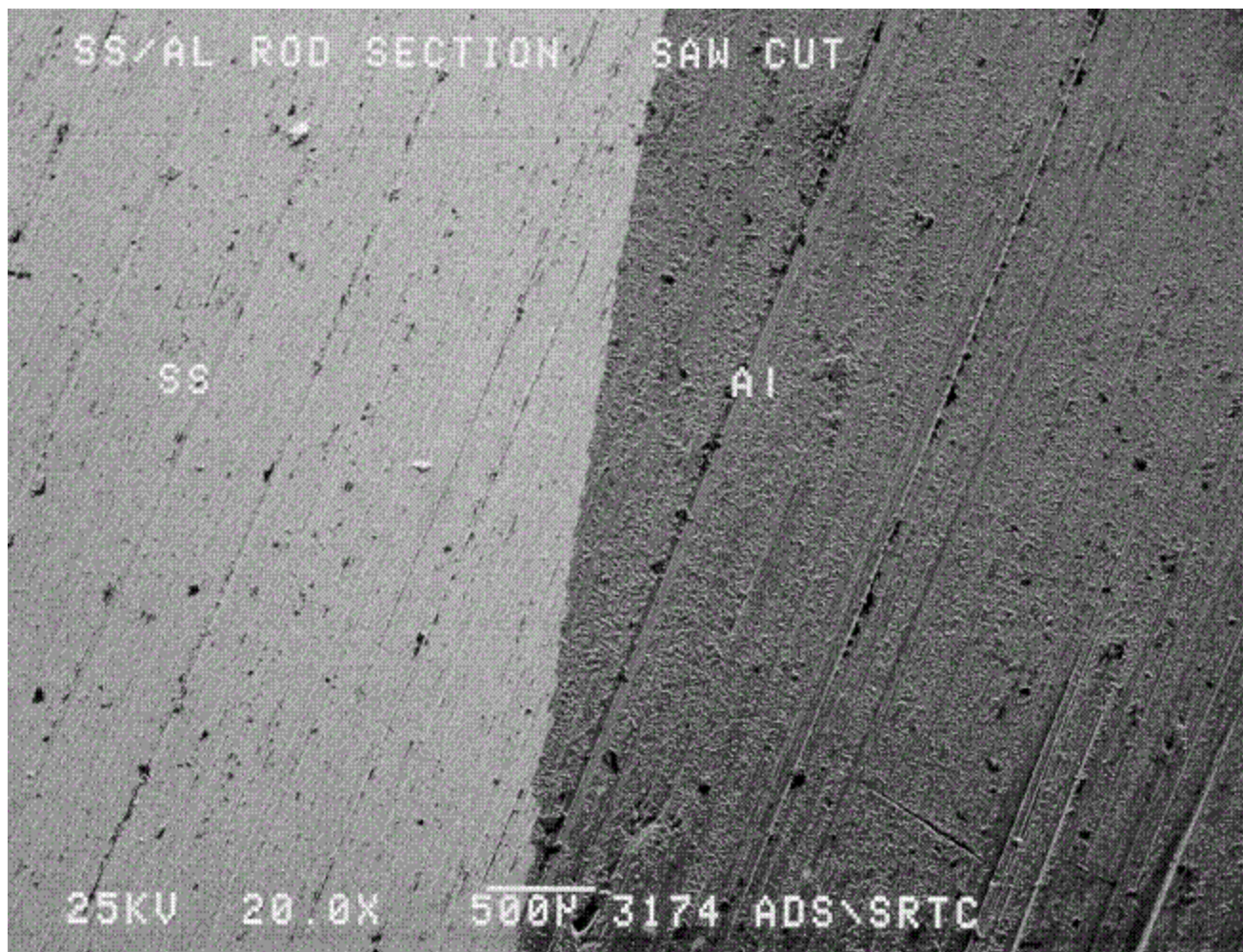
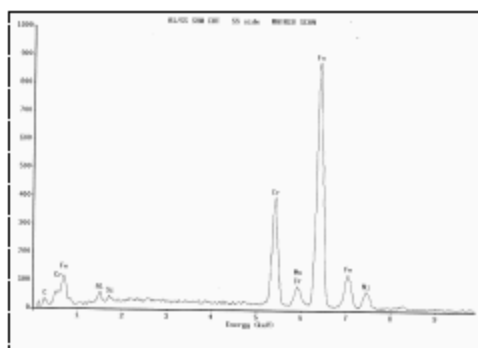**Figure 7. SEM photograph of cut section of inertia weld.**

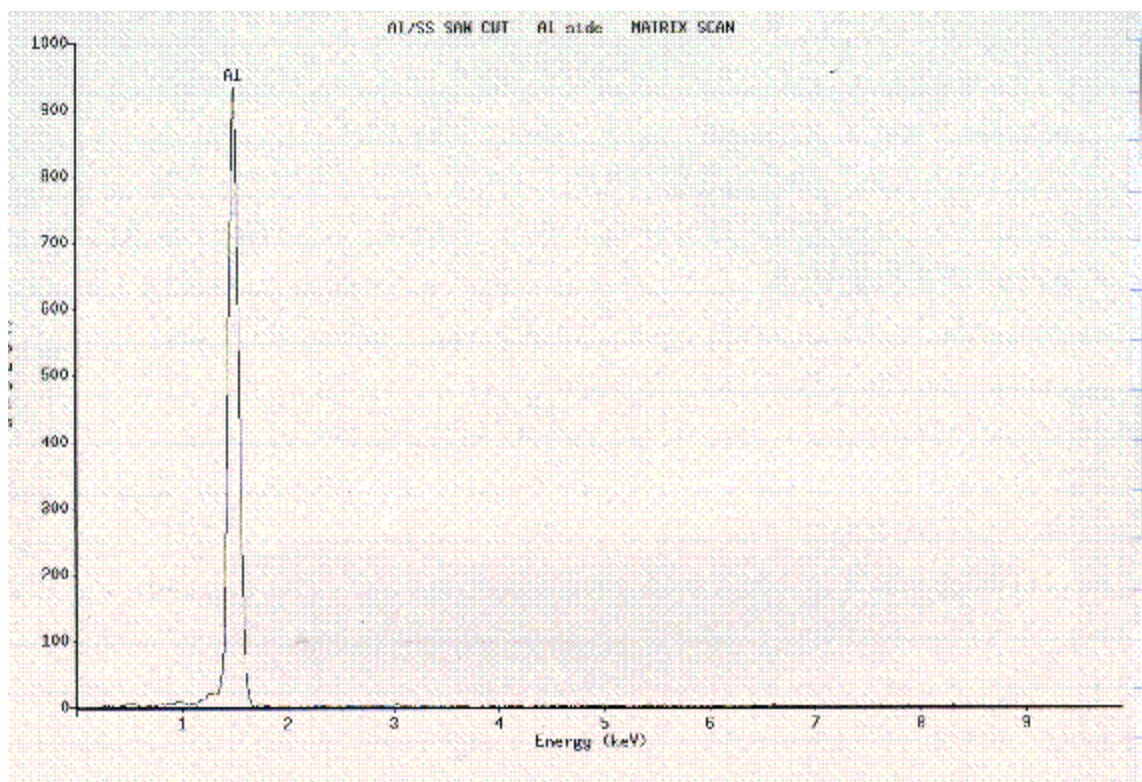**Figure 8. EDS of SS side from cut section.**

Figure 9. EDS of Al side from cut section.

Metallographic Technique Development and Analysis

Metallographic specimens were prepared by mounting a rod section at the Al/SS weld interface, and a section from each parent metal (Al and 304L SS) away from the weld. The mounted Al and SS parent materials were ground and polished for etching using traditional methods for each material. Preparation of the Al/SS interface weld sample involved complexities inherent to the presence of two dissimilar materials in the same mount. A sequence of silicon carbide grinding papers and diamond suspension polishing cloths were coupled with specific values for application force and working time to develop an appropriate interface sample (Table 1). The force and time values indicate the compromise necessary to achieve acceptable quality from preparation of the Al/SS weld specimen.

Table 1. Sample preparation sequence for metallographic analysis.

Grinding/Polishing Sequence	Prep. Time (s)	Application Force (N)
500, 600, 800, 1200, 2400 grit SiC Papers	90 (Each)	100,150,100 (Each)
1 μm Diamond Nap Cloth	240	200, 150, 100
6 μm Diamond Nap Cloth	240	200,150,100

*Note: Application forces vary among the three listed for each preparation step.

Various etchants for the Al/SS interface sample were tested. The need to transfer the final process to the CMR hot cells provided criteria such as an etching sequence that was relatively easy to employ while yielding satisfactory results. As in the grinding and polishing process, the etching of the Al/SS interface specimen involved a certain degree of compromise due to the constituent materials. The etching sequence used involved the application of Poulton's etching solution for the Al section followed by an electrolytic oxalic acid solution for the SS (Table 2).

Table 2. Exposure times and compositions of etchants used in metallographical analysis.

Poulton's Etching Solution (Al etchant)	Oxalic Acid Solution (SS etchant)
50 mL Poulton's Reagent* 40 mL chromic acid solution** 25 mL HNO_3	10 g oxalic acid 100 mL H_2O (6V applied to solution)
Exposure Time: 10 sec.	Exposure Time: 60 sec.

*12 parts HCl, 6 parts HNO_3, 1 part HF, 1 part H_2O

**3 g chromic acid per 10 mL H_2O

Mounted Al and SS parent metal specimens were also prepared using the etchant appropriate for each specific metal. Typical microstructures of the base metals and the inertia welded interface are shown in Figures 10-12. In Figure 10, the observed grain structure indicates that the aluminum alloy was hot rolled during fabrication as seen by the elongated grains in the mid-section. The exterior material of the solid Al cylinder appears to have been worked more extensively than the interior thus leading to the smaller recrystallized grains. Photographs of the stainless steel parent material, Figure 11, are consistent with typical Type 304L stainless steel microstructures. Figure 12 clearly shows the microstructural characteristics of the inertia weld. The flow of aluminum around the welded region and the flash hangover on the samples is characteristic of the inertia welding process.
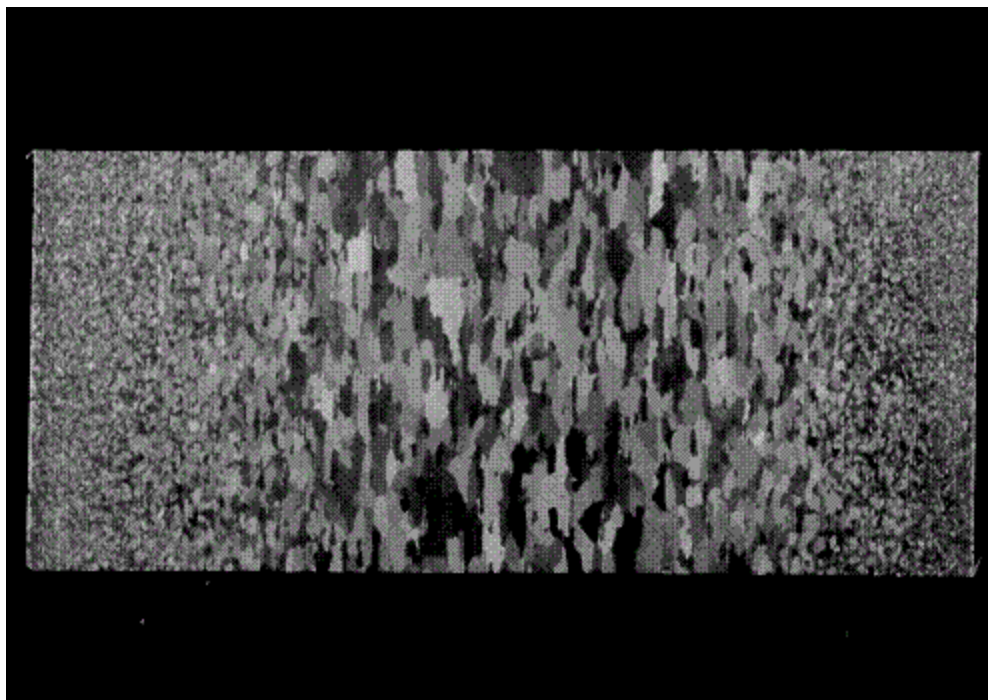
Figure 10. Mounted 6061 T6 aluminum parent material showing elongated grains and recrystallized grains.
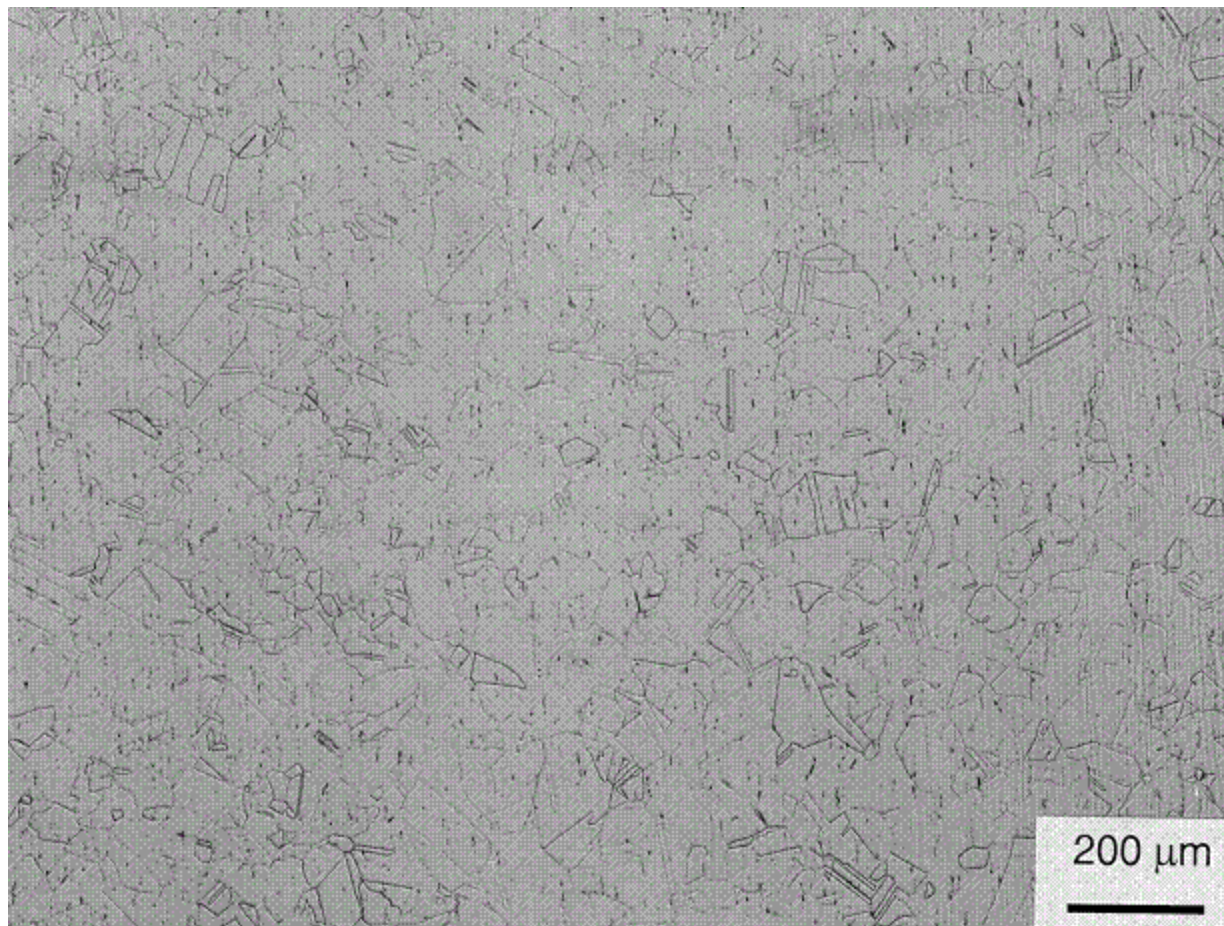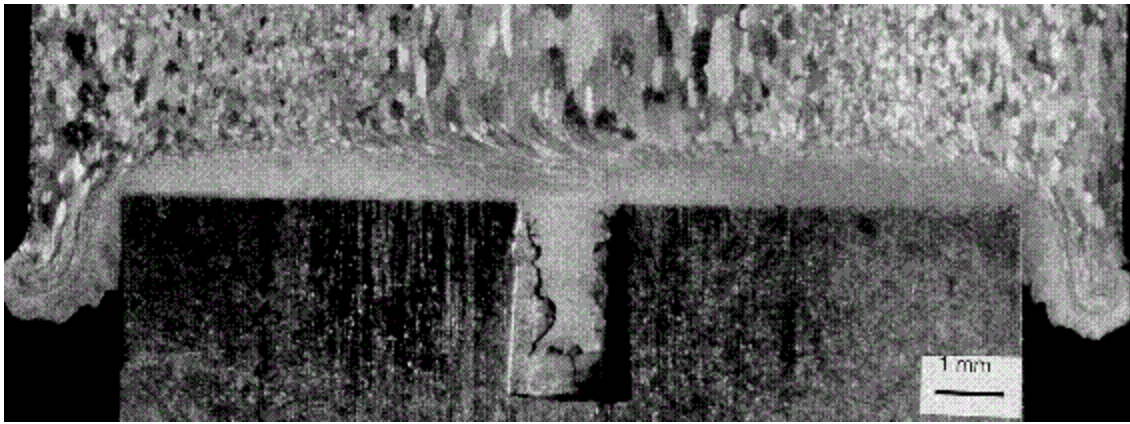

Figure 11. Mounted 304L stainless steel parent material showing normal behavior.

**Figure 12. Mounted inertia welded 6061 T6 aluminum to 304L stainless steel.
Showing the flow of Al material around the SS.**

SEM Analysis

Following etching, the Al/SS interface sample was examined with SEM/EDS to evaluate the Al and SS structure along the inertia weld. Examination of the area surrounding the Al/SS interface revealed the appearance of "ditching" along the grain boundaries of the SS material, Figure 13. The "ditching" was also apparent in the SS parent material and is typical of minor amounts of sensitization. The Al alloy appeared to have a dimpling structure throughout the matrix, probably as a result of the etching sequence. Consequently, the inertia weld sample was ground and polished, then re-submitted for SEM/EDS analysis in an unetched condition.
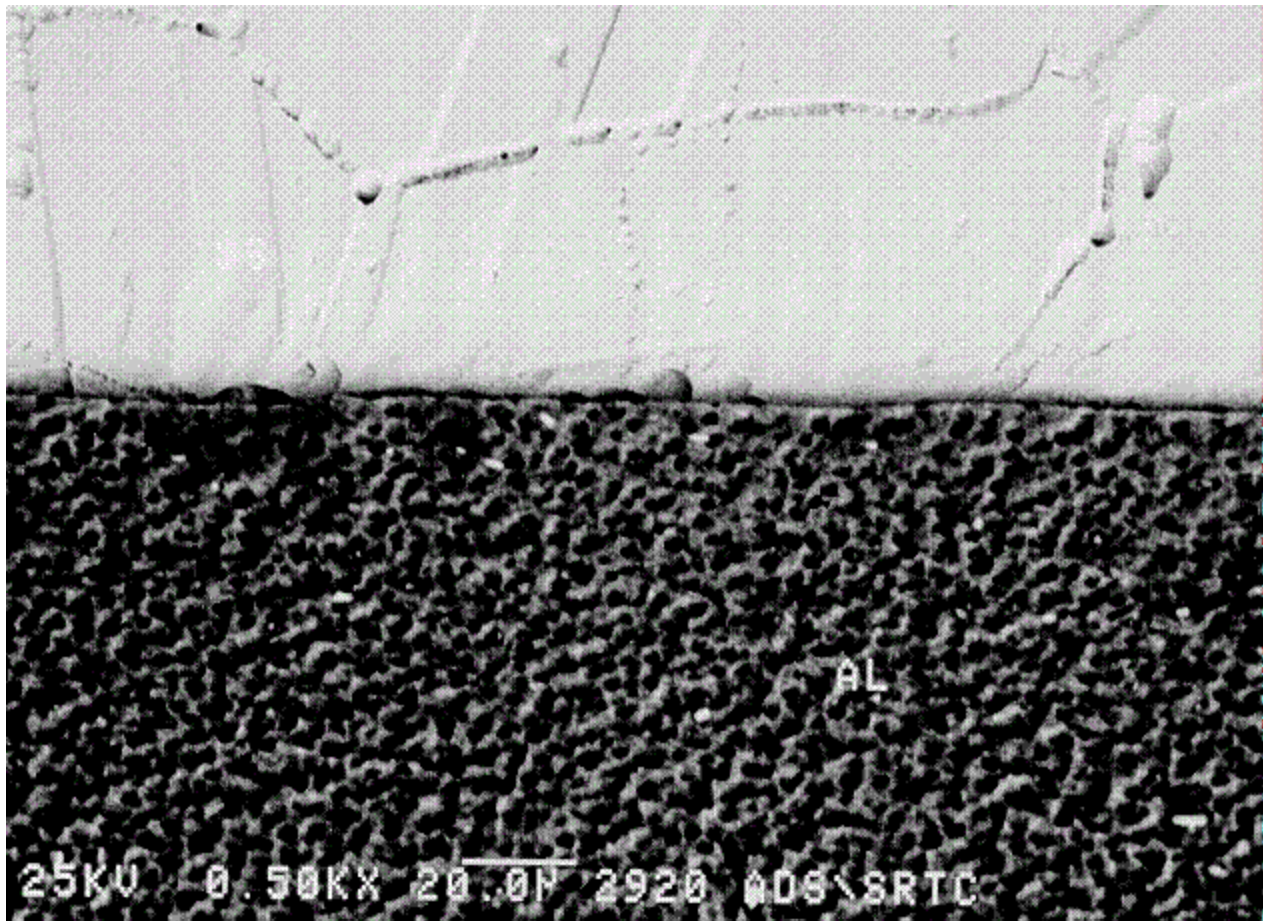
Figure 13. SEM of mounted and etched 6061 T6 Al to 304L stainless steel inertia welded specimen.

SEM examination, using the backscattered electron detector, did not indicate a pattern of particles along the grain boundaries in the SS material. However, a small number of particles were observed in the matrix aligned with the rolling direction, Figure 14. EDS examination of a particle in the matrix revealed the presence of C, Cr, and Mn with trace amounts of O_2 and Al, Figure 15. No impurities in the Al alloy were observed. An EDS analysis across the unetched Al/SS interface is shown in Figures 16 and 17. A distinct separation between the Al and SS was seen and no oxides were detected at the interface.

Figure 14. SEM photograph of stainless steel portion of inertia welded specimen in the unetched condition. Page 28 bottom
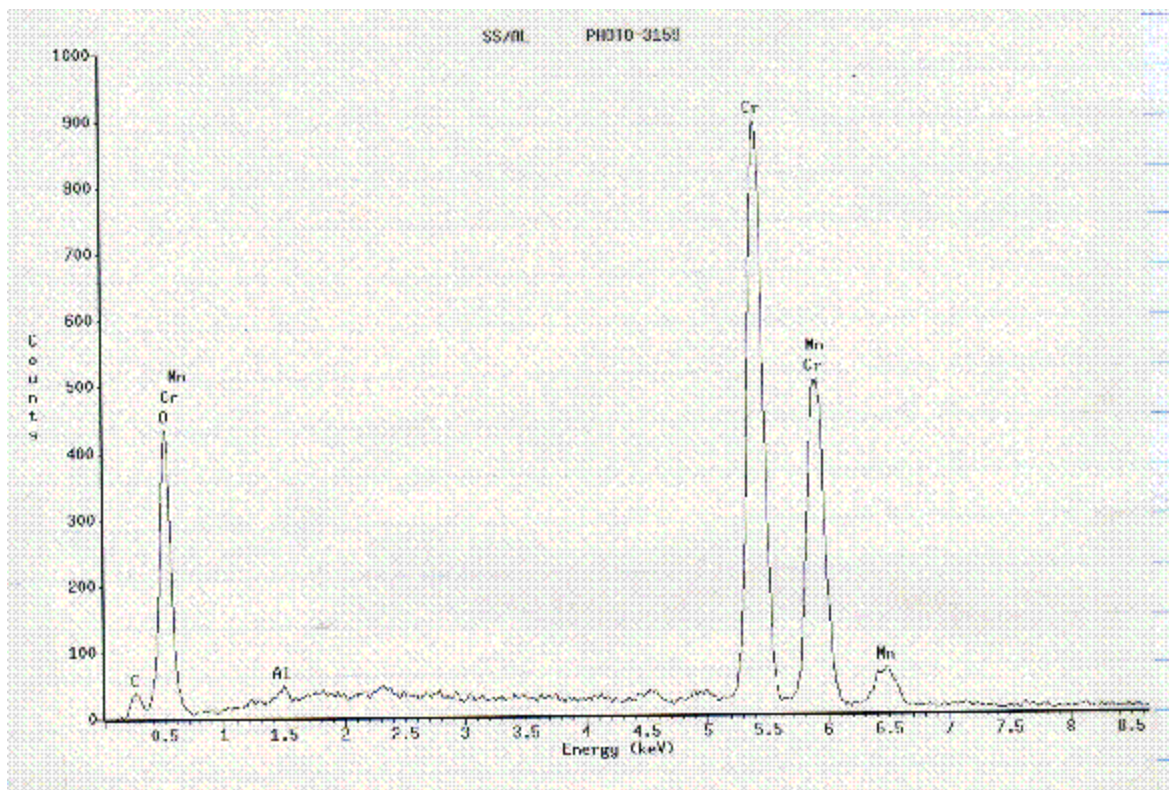
Figure 15. EDS spectrum of particle circled in Figure 14

TEM Analysis

Transmission Electron Microscopy (TEM) was employed to more fully characterize the microstructure of the Al and SS bars - including the HAZ and weld interface regions. With the exception of the interface samples, thin foils were prepared using conventional jet-polishing techniques. (The interface sample was made at LANL using a Gatan Precision Ion Polisher.) The Al samples were prepared using a 25% Nital solution at -20ºC and a voltage of 35Vdc. The SS samples were made using a 4% perchloric acid, 39% butylcellosolve, and 57% methanol solution at -30ºC and 35Vdc. All foils were examined using a JEOL 2010 equipped with a Kevex Sigma EDS system.

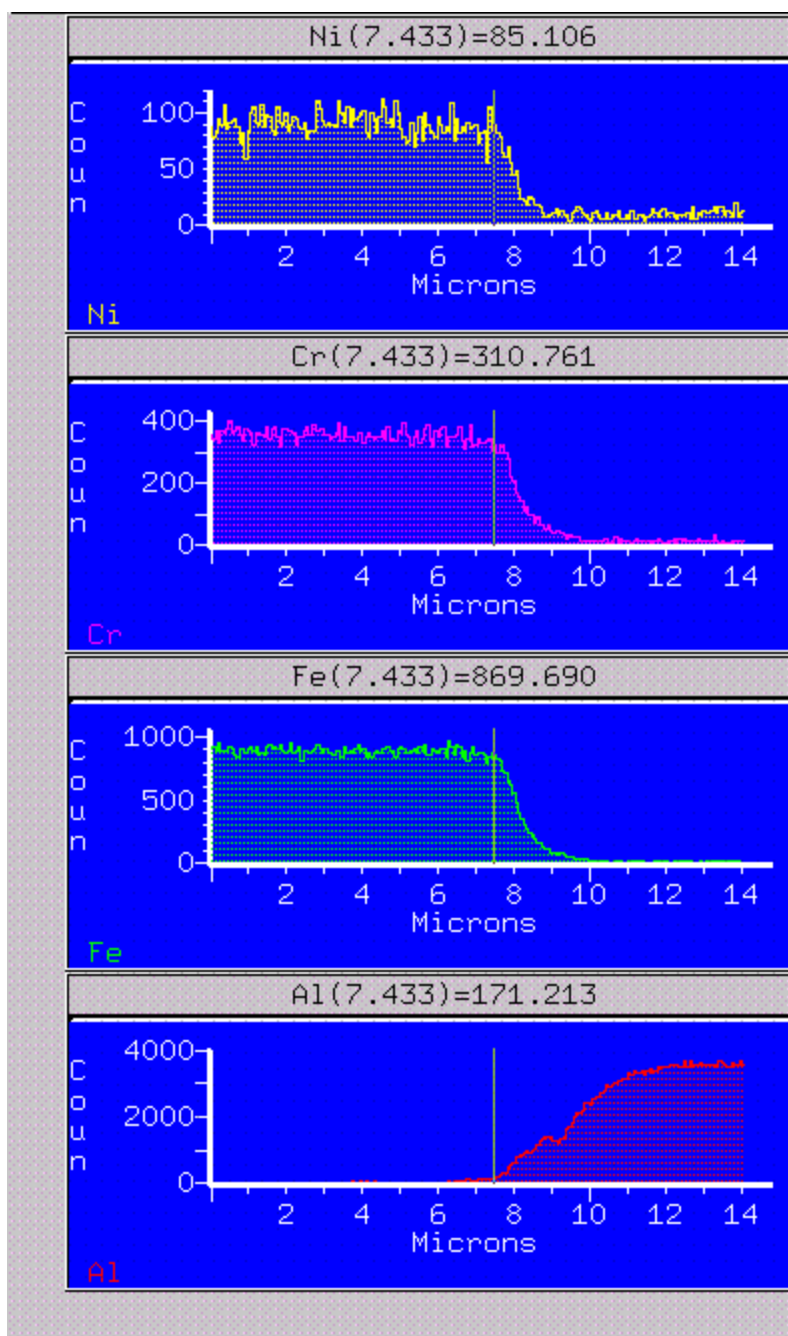**Figure 16. "SEM photograph of mounted and unetched Al/SS inertia weld.**

Figure 17. EDS scans for Fe, Cr, Ni, and Al across surface of mounted and unetched Al/SS inertia weld shown in Figure 16.
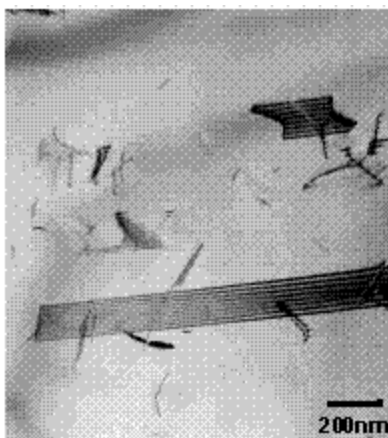
Figure 18. Stacking faults and dislocations in SS base material.

The microstructure of the SS was typical of annealed austenitic stainless steel (Figure 18). Numerous stacking faults, annealing twins, and a very low free-dislocation density were observed. TEM did not reveal the presence of any precipitate species in this material.

The base microstructure of the Al consisted of large, seemingly, equi-axed grains containing a high dislocation density. All foils contained a low number density of 1-2μm sized Si, Mg, and O-containing particles. These inclusions were randomly distributed throughout the material. A coarse constituent phase containing Al, Fe and Si was also observed (Figure 19). This phase was more numerous than the oxide phase and was also observed throughout the Al matrix. Because of limited diffraction data this phase was not identified, however, a constituent phase with similar morphology, namely, α-$Al_{12}Fe_3Si$ was identified in alloy 6061 by Jenski [6]. For clarity purposes the Al, Fe, and Si phase identified in the current study will be identified as α(AlFeSi).

The most abundant precipitate species in the base material was a rod-like dispersoid measuring 0.1 to 0.3μm in size (Figure 20). This phase was observed in the Al matrix, on grain boundaries and, in some cases at the α(AlFeSi)/matrix interface i.e., the α(AlFeSi) served as a nucleation substrate for the "dispersoid" phase (e.g., at arrow in Figure 19). This phase contained Al, Fe, Cr, Si, Mn, and Cu and indexed consistently as a body-centered cubic (bcc) phase with a lattice parameter (a_o) of approximately 12.68Å. A phase containing Fe, based on $Al_9Mn_2Si_{1.8}$ identified by Copper and Robinson [7], was observed in alloy 6013 by Jenski et al. [8]. Although the stoichiometry was never determined, the α(AlFeMnSi) phase in alloy 6013 was bcc with a_o=12.68Å.
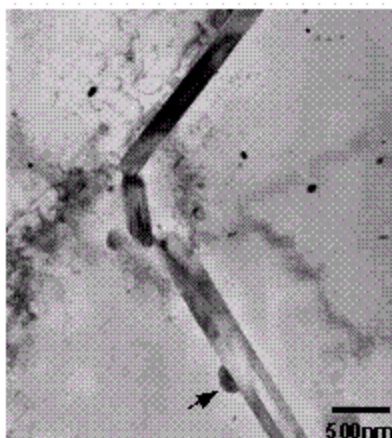

Figure 19. Large α(AlFeSi) constituent particles in the Al.

Additionally, Jensky [6] reported the presence of α-$Al_{12}(Fe,Cr)_3Si$ dispersoids in a alloy 6061 (modified with Cr) with a bcc crystal structure and a_o = 12.6Å. The phase observed in the present study may be a modified form of the above phases with the additions of Mn and Cu.
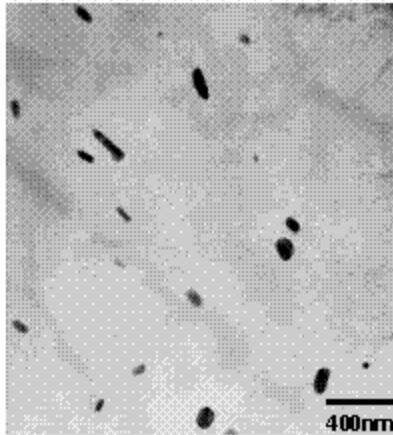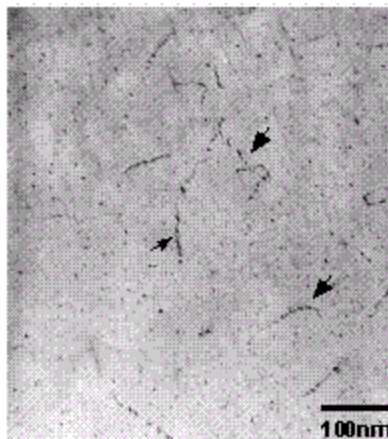

Figure 20. Dispersoid phase in the Al matrix.

Figure 21. β' precipitates in the Al matrix.

The last precipitate species observed in the Al base material is imaged in Figure 21. This phase formed in the matrix <100> and was present as small needles (or parallelepipeds). The morphology and precipitate orientation is consistent with this phase being β', the Mg_2Si intermediatephase [9]. This precipitate species also formed on matrix dislocations in a slightly more "blocky" morphology than within the Al matrix (e.g., at arrows in Figure 21). β' precipitate-free zones were also observed at the high angle boundaries in this alloy.
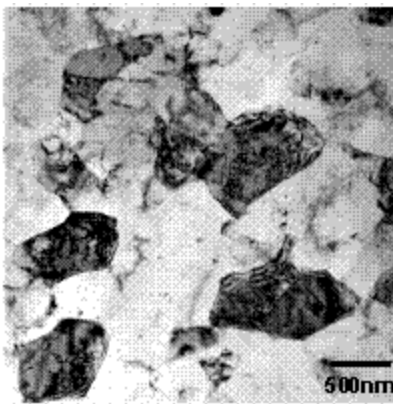
Figure 22. Grain structure in Al HAZ.

In the Heat Affected Zone (HAZ) of the inertia weld, approximately 100μm from the interface, the grain size was much smaller than the base material (Figure 22). Grain diameters ranged from 1-2μm in diameter. Similar to the base material, large Si, Mg, and O-containing particles and the α(AlFeSi) constituent phase were observed in the HAZ. Additionally, large, amorphous SiO_2 particles were found in the matrix. The bcc dispersoid phase observed in the base material was also present in the HAZ.

Another precipitate phase, nearly as numerous as the bcc dispersoid phase, was observed in the HAZ. This phase contained Al, Si, Mg, and Cu and was distributed randomly throughout the matrix (Figure 23). Similar to the bcc dispersoid phase, it appeared to be mostly rod-shaped but the size of the particles was much smaller, i.e., <0.1μm. This phase was very weakly diffracting making identification impossible. However, the phase composition is similar to that of the Q phase which can form in Cu-bearing 6XXX alloys [8]. It is interesting to note when particles of this phase intersected the foil surface they oxidized upon contact with, presumably, the jet-polishing solution. This resulted in oxide eruptions on the surface of the thin foils. Two of these oxidized precipitates can be seen at the arrows in Figure 23. The dark center is the region where the precipitate remains and the lighter annulus is the oxide residue. No evidence of the β' phase was observed in the HAZ.
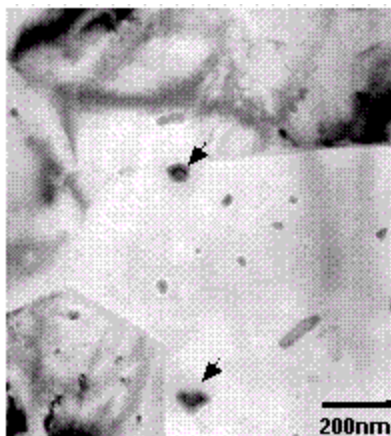

Figure 23. Al, Si, Mg, Cu phase in the Al HAZ.

The interface region can be seen in Figure 24. The interface was reasonably flat with no mixing of Al and SS. This was confirmed by EDS analysis on both sides of the interface. The Al microstructure (grain size, precipitate distribution, etc.) immediately adjacent to the interface appeared the same as in the HAZ. The SS side of the

interface was characterized by a very fine polycrystalline microstructure extending approximately 1μm into the stainless steel base before gradually returning to the nominal SS grain size. The grains in this region measured from about 30 to about 100nm in diameter and were slightly pancaked parallel to the interface.

Precipitates were observed to have nucleated on the interface (e.g. at A in Figure 24) and subsequently grown into the Al matrix. EDS analysis indicated that these precipitates had the same composition as the bcc dispersoid phase observed in the base alloy and HAZ. One further item of note is that there appeared to be a 3-5nm thick, discontinuous amorphous "film" along the Al/SS boundary in some regions (at arrows in Figure 24). Subsequent EDS analysis indicated this narrow region may have been enriched in oxygen.
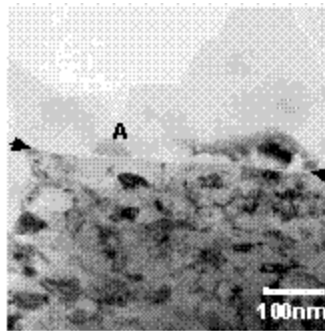

Figure 24. Weld interface. The Al is at the top and SS is at the bottom in this image.

Summary and Conclusions

The 6061 T6 Al inertia welded to 304L samples were shown to exhibit clean, well bonded interfaces. SEM and TEM results indicate little mixing of the materials and few precipitates along the bond interface. These interfacial and near interface microstructures do not contain inclusion or precipitate morphologies that would suggest the presence of a leak path along the interface. The lack of such a path was confirmed by leak testing of ^{3}He filled pressure tubes.

A grinding, polishing and etching technique developed for the unirradiated Al/SS inertia weld was integrated into the analysis of the irradiated Al/SS inertia welds that are located at the LANL CMR hot cells. This metallographic preparation technique for the Al/SS inertia welded samples provides an effective baseline characterization to which the irradiated samples can compare to determine any possible effects on the materials from the irradiation process.

Acknowledgments

References

1. *Welding Handbook: Welding Processes*, "Friction Welding", 8th Edition, pp. 740-761, O'Brien, R.L., American Welding Society, 1991
2. Spindler, D. E., *What Industry Needs to Know about Friction Welding,* Welding Journal, pp. 37-42, March 1994

3. V. R. Ryabov on *Welding of Aluminum Alloys to Steels*, pp. 67-69, Harwood Academic Publishers, Ottawa, Canada, (1988)

4. Wadleigh, A.S., *Bi-Metal Welding of Aluminum*, Interface Welding, Carson, CA

5. M. R. Louthan, Jr., G. R. Caskey, Jr., and A. H. Dexter, *Hydrogen Effects in Aluminum Alloys*, Radiation Effects and Tritium Technology for Fusion Reactors, Vol. IV, p. IV-117, CONF-750989, Oak Ridge National Laboratory, 1976

6. Jenski, R. A., Jr., *Effects of Cr Addition on the Microstructure and Mechanical Behavior of 6061-T6 Continuously Cast and Rolled Redraw Bar*, Mater. Sci. Eng. A 237, pp. 52-64, 1997.

7. Cooper, M. and Robinson, K., *The Crystal Structure of the Ternary Alloy [alpha](AlMnSi)*, Acta Cryst., vol. 20, pp. 614-17, 1966.

8. Jenski, R. A., Jr., Thanaboonsombut, B., and Sanders, T. H., Jr., *The Effect of Iron and Manganese on the Recrystallization Behavior of Hot-Rolled and Solution-Heat-Treated Aluminum Alloy 6013*, Metallurgical and Materials Transactions A, vol. 27A, pp. 19-27, 1996.

9. Smith, W. F., The Effect of Reversion Treatments on Precipitation Mechanisms in an Al-1.35 at. pct Mg_2Si Alloy, Metall. Trans., vol. 4, pp. 2435-40, 1973.